


## AUTHOR QUERY FORM

	<p><b>Journal:</b> Appl. Phys. Lett.</p> <p><b>Article Number:</b> APL19-AR-10398</p>	<p>Please provide your responses and any corrections by annotating this PDF and uploading it to AIP's eProof website as detailed in the Welcome email.</p>
-----------------------------------------------------------------------------------	---------------------------------------------------------------------------------------	------------------------------------------------------------------------------------------------------------------------------------------------------------

Dear Author,

Below are the queries associated with your article; please answer all of these queries before sending the proof back to AIP.

**Article checklist:** In order to ensure greater accuracy, please check the following and make all necessary corrections before returning your proof.

1. Is the title of your article accurate and spelled correctly?
2. Please check affiliations including spelling, completeness, and correct linking to authors.
3. Did you remember to include acknowledgment of funding, if required, and is it accurate?

Location in article	Query / Remark: click on the Q link to navigate to the appropriate spot in the proof. There, insert your comments as a PDF annotation.
<a href="#">AQ1</a>	Dear Author, This second proof is for confirmation only. We cannot accept new corrections at this time. Please do not make additional changes to your proof unless it is to fix an error made by AIP. When we receive your confirmation, your article will be readied for online publication. Thank you.

Thank you for your assistance.

AQ1

# Current induced chiral domain wall motion in CuIr/CoFeB/MgO thin films with strong higher order spin-orbit torques

Cite as: Appl. Phys. Lett. **116**, 000000 (2020); doi: [10.1063/1.5139704](https://doi.org/10.1063/1.5139704)

Submitted: 3 December 2019 · Accepted: 17 February 2020 ·

Published Online: 0 Month 0000



Franziska Martin,<sup>1</sup> Kyujoon Lee,<sup>1,a)</sup> Alexander Kronenberg,<sup>1</sup> Samridh Jaiswal,<sup>1,2</sup> Robert M. Reeve,<sup>1,3</sup> Mariia Filianina,<sup>1,3</sup> Sanghyun Ji,<sup>1,3,4</sup> Myung-Hwa Jung,<sup>4</sup> Gerhard Jakob,<sup>1,3</sup> and Mathias Kläui<sup>1,3</sup>

## AFFILIATIONS

<sup>1</sup>Institute of Physics, Johannes Gutenberg University, 55099 Mainz, Germany

<sup>2</sup>Singulus Technologies AG, 63796 Kahl am Main, Germany

<sup>3</sup>Graduate School of Excellence Materials Science in Mainz, 55128 Mainz, Germany

<sup>4</sup>Department of Physics, Sogang University, Seoul 04107, South Korea

<sup>a)</sup>Author to whom correspondence should be addressed: [kyulee@uni-mainz.de](mailto:kyulee@uni-mainz.de)

## ABSTRACT

We investigate the Dzyaloshinskii–Moriya interaction (DMI) and spin-orbit torque effects in CuIr/CoFeB/MgO heterostructures. To this end, harmonic Hall measurements and current induced domain wall motion experiments are performed. The motion of domain walls at zero applied field due to current demonstrates the presence of DMI in this system. We determine the strength of the DMI to be  $D = +5 \pm 3 \mu\text{J}/\text{m}^2$  and deduce right-handed chirality in domain walls showing a partial Néel type spin structure. To ascertain the torques, we perform a second harmonic measurement to quantify the damping- and field-like current induced effective fields as a function of the magnetization direction. From the angular dependent analysis, we identify non-negligible higher order terms for polar magnetization angles  $\theta > 0$ , which need to be included when considering the effective manipulation of spins by current.

Published under license by AIP Publishing. <https://doi.org/10.1063/1.5139704>

Research into materials suitable for spintronics is crucial to effectively utilize the spins of electrons as information carriers. One example of novel digital data storage concepts is the racetrack memory,<sup>1</sup> which utilizes a series of magnetic domains that store the information and are separated by domain walls that can be moved by electrical currents. There have been observations of fast and synchronous domain wall motion in ultra-thin heterostructures with perpendicular magnetic anisotropy (PMA), which consist of a ferromagnetic layer (FM) sandwiched between a heavy metal (HM) and an oxide layer.<sup>2–4</sup> These systems allow for the efficient manipulation of magnetization due to their structural inversion asymmetry (SIA) combined with a strong spin-orbit coupling. Both properties in combination lead to the generation of spin-orbit torques (SOTs) as well as the presence of the interfacial Dzyaloshinskii–Moriya interaction (DMI).<sup>5–7</sup> The SOTs that allow ultra-efficient and synchronous domain wall motion move the chiral domain walls stabilized by the DMI.<sup>3,4,8</sup> In typical PMA systems, such as Pt/Co/AlOx<sup>2,9,10</sup> and Ta/CoFeB/MgO,<sup>11</sup> the stabilization of Néel domain walls due to DMI, along with the efficient current induced control of the magnetization via SOTs, has been studied.

Here, the inverse spin galvanic effect<sup>12,13</sup> and the spin Hall effect<sup>14,15</sup> are known to be responsible for SOTs.<sup>8</sup> Recently, metallic alloy systems such as Au–W,<sup>16</sup> Au–Cu,<sup>17</sup> Au–Pt,<sup>18</sup> Cu–Bi,<sup>19</sup> Cu–Pb,<sup>20</sup> and Cu–Ir<sup>21,22</sup> have shown large spin Hall effects, which implies efficient charge to spin conversion that can lead to large SOTs. Specifically, the alloy of Cu–Ir has been shown to exhibit a sizeable spin Hall angle (SHA),<sup>21,22</sup> which means that a large charge to spin conversion efficiency can be expected. Previous studies have found a temperature independent SHA in Ir doped Cu (for  $T < 200$  K), the size of which was found to be 0.021 for an iridium concentration of 1%–12%.<sup>21</sup> There have also been studies showing an efficient spin to current conversion in the iridium concentration range of ~40%.<sup>22</sup> However, there have not been studies on the current induced domain wall motion due to the SOTs or a quantification of them in these systems. Thus, in this work, using this composition with efficient spin to current conversion, we investigate domain wall motion in the material stack Cu<sub>60</sub>Ir<sub>40</sub>/Co<sub>20</sub>Fe<sub>60</sub>B<sub>20</sub>/MgO. From the current induced domain wall motion, we extract the strength of the DMI. In order to investigate the main driving force of such domain wall motion, we use second harmonic Hall

63 measurements to provide a quantitative analysis of the SOTs in our  
64 system.

65 The thin  $\text{Cu}_{60}\text{Ir}_{40}(5\text{ nm})/\text{Co}_{20}\text{Fe}_{60}\text{B}_{20}(0.6\text{ nm})/\text{MgO}(3\text{ nm})/\text{Ta}(5\text{ nm})$   
66 film was deposited by magnetron sputtering (Singulus ROTARIS)  
67 onto a thermally oxidized silicon substrate. To obtain PMA, the film  
68 was annealed at  $300^\circ\text{C}$  for 2 h at a pressure of  $10^{-8}$  mbar. The mag-  
69 netic properties were measured using a superconducting quantum  
70 interference device (SQUID) magnetometer. The measured anisotropy  
71 field and saturation magnetization are  $\mu_0 H_k = 0.18 \pm 0.01\text{ T}$   
72 and  $M_s = 5.7 \pm 0.2 \times 10^5\text{ A/m}$ , respectively. Using electron-beam  
73 lithography, we pattern 30 microwires each having dimensions of  
74  $1\ \mu\text{m} \times 30\ \mu\text{m}$  with two pads at the ends of the wires [see Fig. 1(a)]  
75 for the scheme of the domain wall velocity measurement]. For the  
76 second harmonic Hall measurement [see Fig. 2(a)], we pattern a  
77 Hall bar. The current induced domain wall motion experiment is  
78 performed at room temperature with a polar Kerr microscope using  
79 the differential contrast mode. To inject pulses into the microwires,  
80 we used a pulse generator and monitored the transmitted pulses  
81 using an oscilloscope, as illustrated in Fig. 1(a). To move the

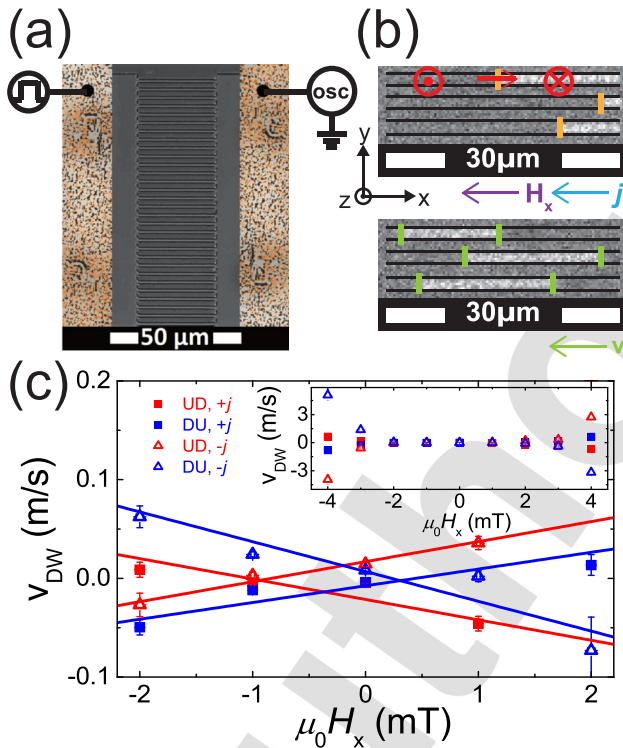


FIG. 1. (a) Microscope image of the microwires with the schematics of the setup for the domain wall (DW) motion. (b) Differential Kerr microscopy images of current induced DW motion at  $H_x = -2\text{ mT}$  before and after 5000 current pulses with an amplitude of  $j = -7.2 \times 10^{11}\text{ A/m}^2$ . Red symbols display the magnetization state. Gray refers to up and white to down magnetization. The orange lines indicate the location of the initialized DWs, and the green lines indicate the moved distance. (c) Current induced DW velocity as a function of the applied in-plane field  $H_x$ . The lines represent linear fits to the shown data points. The inset shows the same data with a larger in-plane field range from  $-4\text{ mT}$  to  $4\text{ mT}$ . The experiment was done at room temperature. Red data refer to up-down (UD) DWs, and blue data to down-up (DU) DWs.

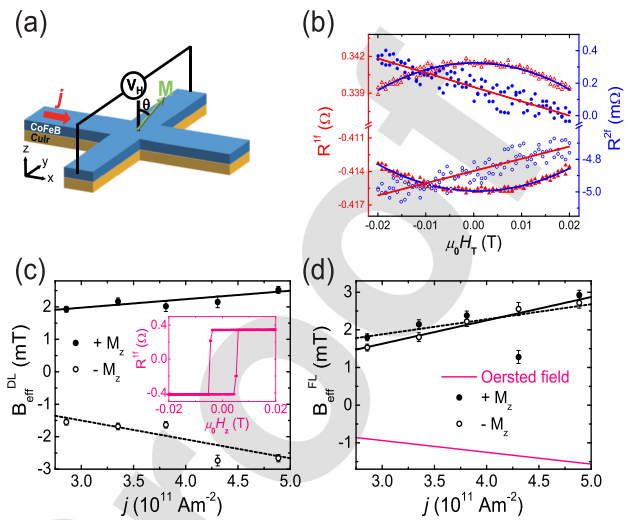


FIG. 2. (a) Schematic of the second harmonic measurement in a Hall bar geometry. (b) First (red) and second harmonic Hall resistances (blue) as a function of an external field along the transverse  $y$ -direction. Filled (empty) symbols display an initial magnetization configuration along the  $+z$  ( $-z$ ) direction. The solid lines are the fit lines used for the analysis. (c), (d) DL and FL effective fields plotted vs the applied current density  $j$ . Solid (dashed) lines refer to a linear fit including the  $+z$  ( $-z$ ) values. The inset in (c) shows the first harmonic Hall resistance as a function of an applied field along the  $z$ -direction. The pink line in (d) depicts the Oersted field. All data represented here are measured at room temperature.

nucleated domain walls, a series of either positive or negative current pulses is applied. The domain wall displacement is imaged via polar Kerr microscopy by subtracting a background image of the nucleated domain walls from the one after the current induced motion [for examples, see Fig. 1(b)]. Depending on the amplitude of the external in-plane field, a series of 20 ns current pulses was sent through the wires, ranging from 100 to 50 000. The ratio between the domain wall displacement and the total pulse time corresponds to a single domain wall velocity. For the analysis, we use the fact that the domain wall only moves during the pulse injection time. The injected current density when assumed to be distributed equally for all wires is calculated to be  $j = \pm 7.2 \times 10^{11}\text{ A/m}^2$ .

The SOTs were quantified by a second harmonic Hall measurement.<sup>9,23,24</sup> Since a temperature dependent analysis can reveal the mechanisms and origins of the SOTs, we measured the SOTs at  $T = 10$  and  $300\text{ K}$ . The SOTs were determined for different magnetization tilt angles  $\theta$  by measuring different magnetic field ranges.<sup>25</sup>

In Fig. 1(c), the in-plane field dependence of the average domain wall velocity  $v_{\text{DW}}$  with the corresponding standard error is displayed. We consider domain wall velocities for the cases when more than 50% of the initialized domain walls have moved since each domain wall has a different depinning originating from edge roughness and defects due to the device fabrication. In Fig. 1(b), you can see an example of the domain wall motion along the technical current direction, which is the direction against the electron flow. This underlies the fact that we move domain walls by SOTs, as spin-transfer torque would move walls along the electron flow direction.<sup>26</sup> For the domain wall to be moved by SOTs, a Néel component in the domain wall needs to be present.<sup>4,27</sup> Thus, when the in-plane field compensates the Néel wall component,

111 this marks the stopping field when the domain wall velocity is zero.  
 112 Accordingly, if DMI is present in our system, the stopping field is  
 113 non-zero and independent of the current direction. For chiral  
 114 up-down and down-up domain walls, the sign is expected to be oppo-  
 115 site, while the absolute values should be the same. The magnitude of  
 116 the DMI can be extracted from these stopping fields. In accordance to  
 117 a simple 1D model, we expect a linear relation between the domain  
 118 wall velocity and the applied in-plane field.<sup>11</sup> Therefore, in the field  
 119 range  $-2 \text{ mT} \leq \mu_0 H_x \leq 2 \text{ mT}$ , we perform linear fits to determine  
 120 the value of the stopping field. This field matches the effective  
 121 DMI field  $|\mu_0 H_{\text{DMI}}|$ . By averaging the absolute value of the two inter-  
 122 section points for up-down and down-up domain walls, we obtain  
 123  $|\mu_0 H_{\text{DMI}}| = 0.6 \pm 0.3 \text{ mT}$ . This value leads to a DMI constant of  
 124  $D = 5 \pm 3 \mu\text{J}/\text{m}^2$  according to the relation  $D = \mu_0 H_{\text{DMI}} M_s \Delta$ ,<sup>28</sup> where  
 125  $\Delta = \sqrt{A/K_{\text{eff}}}$ <sup>29</sup> is the domain wall width, while  $A$  is the exchange  
 126 stiffness and  $K_{\text{eff}} = \mu_0 H_k M_s / 2$  is the effective anisotropy constant  
 127 in line with the Stoner-Wohlfarth model.<sup>30</sup> We have used  
 128  $A = 10^{-11} \text{ J/m}$  from the literature.<sup>11,31</sup> For the larger field range,  
 129  $2 \text{ mT} \leq |\mu_0 H_x|$  [see the inset of Fig. 1(c)], an increase in the domain  
 130 wall velocity can be observed. To estimate whether the domain walls  
 131 in our system are fully Néel-type, we calculate the critical DMI con-  
 132 stant  $D_c = 4\Delta K_{\text{shape}}/\pi = 34 \mu\text{J}/\text{m}^2$ <sup>28</sup> with the shape anisotropy  $K_{\text{shape}}$   
 133  $= N_x \mu_0 M_s^2 / 2 = (\ln 2 t_{\text{FM}} / \pi \Delta) \mu_0 M_s^2 / 2$ <sup>32</sup> relevant for the domain wall.  
 134 In order to calculate the shape anisotropy of the domain wall, one has  
 135 to consider the demagnetization tensor component  $N_x$ . Here, the ratio  
 136 between the thickness of the ferromagnetic layer  $t_{\text{FM}}$  and the domain  
 137 wall width  $\Delta$  is important. Since the measured DMI constant is smaller  
 138 than the critical DMI value  $D < D_c$ , we expect a domain wall spin  
 139 configuration which is neither completely Néel nor fully Bloch. By  
 140 observing a chiral nucleation of reversed domains,<sup>33</sup> we deduce right-  
 141 handed chiral domain walls with a partly Néel configuration in our  
 142 system that corresponds to a positive DMI constant. A recent study of  
 143 the DMI via Brillouin light scattering in the similar multilayer system  
 144 Ir/CoFeB/MgO has reported a positive DMI constant.<sup>34</sup> This agree-  
 145 ment with our sign of the DMI constant indicates that the 5d-3d  
 146 orbital hybridization<sup>35</sup> with the Ir atoms is the likely underlying mech-  
 147 anism for an enhanced DMI.

148 Since the main driving force of the domain wall motion in the  
 149 above measured system is SOT, we measured the SOTs via second  
 150 harmonic Hall measurements.<sup>9,23-25</sup> We determined the current  
 151 induced effective fields generated by the field-like (FL) and damping-  
 152 like (DL) torques. The first and second harmonic signals of the Hall  
 153 voltage are measured, as shown in Fig. 2(a), while scanning the mag-  
 154 netic fields along the transverse ( $y$ ),  $H_T$ , and longitudinal ( $x$ ),  $H_L$ ,  
 155 directions. We are able to measure the FL and DL components of the  
 156 SOT induced effective fields depending on the applied in-plane field  
 157 direction. In the inset of Fig. 2(c), the magnetic hysteresis loop mea-  
 158 sured via the anomalous Hall effect is displayed, showing a square  
 159 shape and thus indicating a strong PMA in the film.

160 Figure 2(b) shows the representative graphs of the first harmonic  
 161 resistance,  $R^{1f}$ , and the second harmonic resistance,  $R^{2f}$ , signals when  
 162 the in-plane field is applied along the transverse direction for a low in-  
 163 plane field range, where  $R^{1f}$  shows a quadratic and  $R^{2f}$  a linear behav-  
 164 ior. In Figs. 2(c) and 2(d), we present the measured effective fields for  
 165 small polar angles of the magnetization  $\theta \ll 1^\circ$ .<sup>23,24</sup> The applied in-  
 166 plane field range is chosen so that the magnetization tilt angle  $\theta$  will

not exceed  $1^\circ$ , thus maintaining a single domain state. From the  
 relation,<sup>24</sup>

$$B_{\text{eff}}^{\text{DL/FL}} = -2 \frac{(B_{L/T} \pm 2\zeta B_{T/L})}{1 - 4\zeta^2}; \quad (1)$$

we can extract the effective fields, where  $\zeta = R_{\text{PHE}}/R_{\text{AHE}}$  corresponds  
 to the ratio between the planar Hall resistance ( $R_{\text{PHE}}$ ) and the anomalous  
 Hall resistance ( $R_{\text{AHE}}$ ), while  $B_{L/T} = \left( \frac{\partial R^{2f}}{\partial H_{L/T}} / \frac{\partial R^{1f}}{\partial H_{L/T}} \right) \Big|_{\vec{H} \parallel \vec{x}/\vec{y}}$

consists of the first derivative of the second harmonic signal and the  
 second derivative of the first harmonic signal. The  $\pm$  sign corresponds  
 to the case when the magnetization is saturated in the  $\pm z$  direction.  
 The dependencies of the extracted FL and DL effective fields on  
 the current density  $j$  are plotted in Figs. 2(c) and 2(d). As expected  
 from symmetry, the DL effective field is found to be odd with the  
 inversion of the magnetization, while the FL effective field is even.<sup>9,24</sup>  
 In order to evaluate the effective field per current density, a linear fit  
 was performed and the measured effective fields are found to be  
 $B_{\text{eff}}^{\text{DL}} = 0.4 \pm 0.1 \text{ mT}/10^{11} \text{ Am}^{-2}$  and  $B_{\text{eff}}^{\text{FL}} = 0.5 \pm 0.2 \text{ mT}/10^{11} \text{ Am}^{-2}$ .  
 Since the  $B_{\text{eff}}^{\text{FL}}$  effective field is in the direction transverse to the applied  
 current, the contribution from the Oersted field induced by the applied  
 current needs to be taken into account. It was calculated to be  
 $\mu_0 H_{\text{Oe}} = -0.31 \text{ mT}/10^{11} \text{ Am}^{-2,24}$  and is illustrated as a pink line in  
 Fig. 2(d). As the Oersted field is opposite in direction to the FL effective  
 field, its absolute value has to be added to the measured  $B_{\text{eff}}^{\text{FL}}$  value to  
 obtain the FL effective field  $B_{\text{eff}}^{\text{FL}} = 0.8 \pm 0.2 \text{ mT}/10^{11} \text{ Am}^{-2}$  induced by  
 the SOTs.<sup>24</sup> At  $T = 10 \text{ K}$ , we obtain  $B_{\text{eff}}^{\text{DL}} = 1.58 \pm 0.02 \text{ mT}/10^{11} \text{ Am}^{-2}$   
 and  $B_{\text{eff}}^{\text{FL}} = 0.43 \pm 0.01 \text{ mT}/10^{11} \text{ Am}^{-2}$ . Since the low temperature data  
 have a better signal-to-noise ratio than the high temperature data, we  
 observe different relative errors at two different temperatures. By  
 observing a decrease in the DL torque and an increase in the FL torque  
 with increasing temperature and thus different temperature dependen-  
 ces, we likely infer different origins for the torques. To compare our  
 results with the previously reported values of the SHA in CuIr films, we  
 calculate the effective SHA to be  $\vartheta_{\text{SH}} = B_{\text{eff}}^{\text{DL}} 2|e|M_s t_{\text{FM}}/\hbar^4$  assuming  
 that  $B_{\text{eff}}^{\text{DL}}$  is solely due to the spin Hall effect and assuming transparent  
 interfaces between the CuIr and the CoFeB. Here,  $e$  is the electron  
 charge,  $t_{\text{FM}}$  is the thickness of the ferromagnetic layer, and  $\hbar$  is the  
 reduced Planck constant. At room temperature, we obtain  $\vartheta_{\text{SH}}^{300\text{K}}$   
 $= 0.004 \pm 0.001$ , while at 10 K, we extract  $\vartheta_{\text{SH}}^{10\text{K}} = 0.0160 \pm 0.0006$ . For  
 a low iridium concentration ranging from 1% to 12%, a temperature  
 independent value of 0.021 has been previously claimed from measure-  
 ments in a non-local spin valve geometry.<sup>21</sup>

Recently, an analysis showed that the angular dependence of the  
 SOTs needs to be studied in order to understand the mechanism of  
 how the current induced effective field can be applied in domain  
 walls.<sup>25</sup> Therefore, we have measured the polar angular dependence of  
 the SOTs in our system. Figures 3(a) and 3(b) display the first and  
 second harmonic Hall resistances for a larger field range  
 $|\mu_0 H_{L/T}| \leq 0.4 \text{ T}$ . Here, we apply the magnetic field with an out-of-  
 plane tilt of  $\theta = 83^\circ$  to avoid multi-domain formation during the  
 measurement. Accordingly, we apply an analysis method that is valid  
 for an intermediate regime of the polar magnetization angle  $\theta$  before  
 the in-plane saturation state is reached.<sup>9</sup> A full description of the anal-  
 ysis can be found in the supplementary material. In Fig. 3(c), the cur-  
 rent induced effective field components are plotted vs the polar



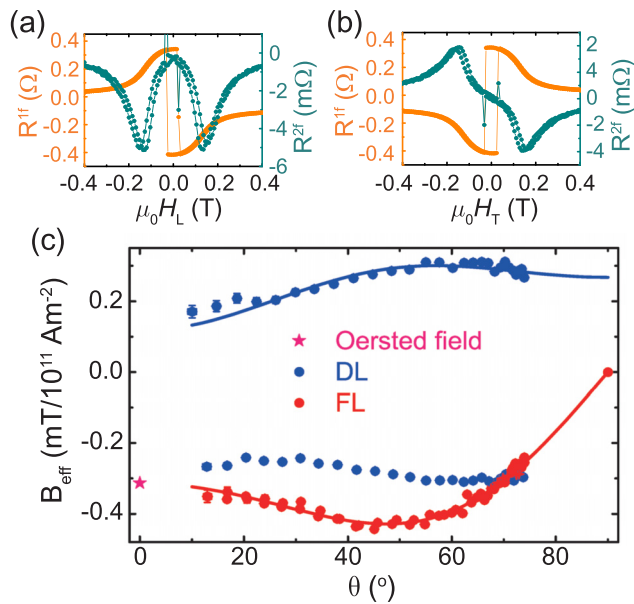


**FIG. 3.** (a) and (b) First and second harmonic Hall resistances as a function of the applied field along the longitudinal/transverse direction. (c) Current induced effective fields as a function of the polar magnetization angle measured at room temperature at a current density of  $j = 2.86 \times 10^{11} \text{ A/m}^2$ . The solid lines represent the fits to the measurement points in accordance with formulas (2) and (3).

219 magnetization angle  $\theta$  measured at room temperature at a current  
 220 density of  $j = 2.86 \times 10^{11} \text{ A/m}^2$ . For the FL component, one addi-  
 221 tionally has to consider the Oersted field contribution that is depicted  
 222 by a pink star in Fig. 3(c). Within the intermediate  $\theta$  model,<sup>9</sup> the FL  
 223 and DL effective fields can be described by the following formulas:

$$B_{\text{eff}}^{\text{FL}} = -\cos\theta \cdot (T_0^{\perp} + T_2^{\perp} \cdot \sin^2\theta + T_4^{\perp} \cdot \sin^4\theta), \quad (2)$$

$$B_{\text{eff}}^{\text{DL}} = (T_0^{\parallel} + T_2^{\parallel} \cdot \sin^2\theta + T_4^{\parallel} \cdot \sin^4\theta). \quad (3)$$

224 The solid lines in Fig. 3(c) represent the fits to the measurement points  
 225 in accordance with formulas (2) and (3). By extracting the slope of these  
 226 single fit parameters plotted against the current density  $j$ , we obtain the  
 227 general effective field parameters normalized to the current density.  
 228 The FL torque parameters are  $T_0^{\perp} = 0.09 \pm 0.03 \text{ mT}/10^{11} \text{ Am}^{-2}$ ,  $T_2^{\perp}$   
 229  $= 1.2 \pm 0.1 \text{ mT}/10^{11} \text{ Am}^{-2}$ , and  $T_4^{\perp} = -0.5 \pm 0.1 \text{ mT}/10^{11} \text{ Am}^{-2}$ .  
 230 For the DL torque, we extract  $T_0^{\parallel} = 0.1 \pm 0.1 \text{ mT}/10^{11} \text{ Am}^{-2}$ ,  $T_2^{\parallel}$   
 231  $= 0.5 \pm 0.4 \text{ mT}/10^{11} \text{ Am}^{-2}$ , and  $T_4^{\parallel} = -0.4 \pm 0.3 \text{ mT}/10^{11} \text{ Am}^{-2}$ . By  
 232 considering both analysis methods, we obtain a full angular dependence  
 233 of the current induced effective FL and DL components. Here,  
 234 we note that the second and third higher order terms of the SOT are  
 235 very important in terms of magnitude compared to the first term.  
 236 Thus, a careful analysis is required when using the measured SOT values  
 237 to understand the dynamics of the different parts of the spin texture  
 238 in a domain wall.<sup>25</sup> From the description of Ref. 25, we calculated the  
 239 average effective SOT field acting on each spin in the DW by

$$B_{\text{DL,FL}}^{\text{avg}} = \frac{1}{\pi\lambda} \int \frac{B_{\text{DL,FL}}(\vartheta(x))}{\cosh\left(\frac{x-X}{\lambda}\right)} dx, \quad (4)$$

where  $H_{\text{DL,FL}}(\vartheta(x))$  is the function of the angular dependence of the  
 240 effective field. From the equation, the calculated  $B_{\text{DL}}^{\text{avg}}$  and  $B_{\text{FL}}^{\text{avg}}$   
 241 are  $0.19 \pm 0.06 \text{ mT}/10^{11} \text{ Am}^{-2}$  and  $0.09 \pm 0.02 \text{ mT}/10^{11} \text{ Am}^{-2}$ , respec-  
 242 tively, which shows that the angular dependence needs to be taken into  
 243 account when considering the SOT effective fields acting on DWs.  
 244

In conclusion, we observed the current induced domain wall  
 245 motion in the especially designed multilayer system CuIr/CoFeB/  
 246 MgO. We choose the specific composition Cu<sub>60</sub>Ir<sub>40</sub> with a high spin to  
 247 current conversion to obtain maximally large SOTs in combination  
 248 with PMA.<sup>22</sup> Using this stack, we determined the DMI strength in our  
 249 system to be  $D = +5.0 \pm 3 \mu\text{J}/\text{m}^2$ . The measured DMI value implies a  
 250 formation of partial Néel walls that are necessary for domain wall  
 251 motion by SOTs. Since the SOTs are the driving force to move domain  
 252 walls here, we extracted the FL and DL components of the SOTs by  
 253 the second harmonic Hall measurements. The measurement of the  
 254 SOTs in two different regimes demonstrates the presence of a strong  
 255 angular dependence of the torques on the magnetization direction. In  
 256 particular, our measurement reveals strong higher order terms of both  
 257 FL and DL torques that are often neglected but need to be taken into  
 258 account when calculating the SOTs acting on spin structures such as  
 259 domain walls.  
 260

See the [supplementary material](#) for the atomic force microscopy  
 261 measurements for the surface roughness information and calculations  
 262 for the angular dependent SOT measurements.  
 263  
 264

We acknowledge G. Karnad for helpful discussions. We  
 265 acknowledge support from the Graduate School of Excellence  
 266 Materials Science in Mainz (MAINZ) GSC 266, MaHoJeRo (DAAD  
 267 Spintronics Network, Project No. 57334897), and the German  
 268 Research Foundation (in particular, SFB TRR 173 Spin+X, in  
 269 particular Project A01 Project No. 290319996/TRR173). K.L.  
 270 acknowledges the European Union's Horizon 2020 Research and  
 271 Innovation Programme under Marie Skłodowska-Curie Grant  
 272 Agreement Standard EF No. 709151 and we thank start-up financing  
 273 and 3D MAGIC (No. ERC-2019-SyG 856538).  
 274  
 275

## REFERENCES

- 276 <sup>1</sup>S. Parkin and S.-H. Yang, *Nat. Nanotechnol.* **10**, 195 (2015).
- 277 <sup>2</sup>I. M. Miron, T. A. Moore, H. Szambolics, L. D. Buda-Predbeanu, S. Auffret, B.  
 278 Rodmacq, S. Pizzini, J. Vogel, M. Bonfim, A. Schuhl, and G. Gaudin, *Nat.*  
 279 *Mater.* **10**, 419 (2011).
- 280 <sup>3</sup>K.-S. Ryu, L. Thomas, S.-H. Yang, and S. Parkin, *Nat. Nanotechnol.* **8**, 527  
 281 (2013).
- 282 <sup>4</sup>S. Emori, U. Bauer, S.-M. Ahn, E. Martinez, and G. S. D. Beach, *Nat. Mater.*  
 283 **12**, 611 (2013).
- 284 <sup>5</sup>T. Moriya, *Phys. Rev.* **120**(1), 91 (1960).
- 285 <sup>6</sup>I. Dzyaloshinsky, *J. Phys. Chem. Solids* **4**(4), 241 (1958).
- 286 <sup>7</sup>A. Crepieux and C. Lacroix, *J. Magn. Magn. Mater.* **182**, 341 (1998).
- 287 <sup>8</sup>A. Manchon, J. Zelezny, I. M. Miron, T. Jungwirth, J. Sinova, A. Thiaville, K.  
 288 Garello, and P. Gambardella, *Rev. Mod. Phys.* **91**, 035004 (2019).
- 289 <sup>9</sup>K. Garello, I. M. Miron, C. O. Avci, F. Freimuth, Y. Mokrousov, S. Blügel, S.  
 290 Auret, O. Boulle, G. Gaudin, and P. Gambardella, *Nat. Nanotechnol.* **8**, 587  
 291 (2013).
- 292 <sup>10</sup>R. Lo Conte, G. V. Karnad, E. Martinez, K. Lee, N.-H. Kim, D.-S. Han, J.-S.  
 293 Kim, S. Prenzel, T. Schulz, C.-Y. You, H. J. M. Swagten, and M. Kläui, *AIP*  
 294 *Adv.* **7**, 065317 (2017).
- 295 <sup>11</sup>R. Lo Conte, E. Martinez, A. Hrabec, A. Lamperti, T. Schulz, L. Nasi, L.  
 296 Lazzarini, R. Mantovan, F. Maccherozzi, S. S. Dhesi, B. Ocker, C. H. Marrows,  
 297 T. A. Moore, and M. Kläui, *Phys. Rev. B* **91**, 014433 (2015).
- 298

- 299 <sup>12</sup>V. M. Edelstein, *Solid State Commun.* **73**, 233 (1990). 323
- 300 <sup>13</sup>S. D. Ganichev, E. L. Ivchenko, V. V. Bel'kov, S. A. Tarasenko, M. Sollinger, D. 324
- 301 Weiss, W. Wegscheider, and W. Pretti, *Nature* **417**, 153 (2002). 325
- 302 <sup>14</sup>J. Sinova, S. O. Valenzuela, J. Wunderlich, C. H. Back, and T. Jungwirth, *Rev.* 326
- 303 *Mod. Phys.* **87**(4), 1213 (2015). 327
- 304 <sup>15</sup>J. E. Hirsch, *Phys. Rev. Lett.* **83**(9), 1834 (1999). 328
- 305 <sup>16</sup>P. Laczkowski, J.-C. Rojas-Sánchez, W. Savero-Torres, H. Jaffès, N. Reyren, C. 329
- 306 Deranlot, L. Notin, C. Beigné, A. Marty, J.-P. Attané, L. Vila, J.-M. George, and 330
- 307 A. Fert, *Appl. Phys. Lett.* **104**, 142403 (2014). 331
- 308 <sup>17</sup>L. K. Zou, S. H. Wang, Y. Zhang, J. R. Sun, J. W. Cai, and S. S. Kang, *Phys. Rev.* 332
- 309 *B* **93**, 014422 (2016). 333
- 310 <sup>18</sup>M. Obstbaum, M. Decker, A. K. Greitner, M. Haertinger, T. N. G. Meier, M. 334
- 311 Kronseider, K. Chadova, S. Wimmer, D. Ködderitzsch, H. Ebert, and C. H. 335
- 312 Back, *Phys. Rev. Lett.* **117**, 167204 (2016). 336
- 313 <sup>19</sup>Y. Niimi, Y. Kawanishi, D. H. Wei, C. Deranlot, H. X. Yang, M. Chshiev, T. 337
- 314 Valet, A. Fert, and Y. Otani, *Phys. Rev. Lett.* **109**, 156602 (2012). 338
- 315 <sup>20</sup>Y. Niimi, H. Suzuki, Y. Kawanishi, Y. Omori, T. Valet, A. Fert, and Y. Otani, 339
- 316 *Phys. Rev. B* **89**, 054401 (2014). 340
- 317 <sup>21</sup>Y. Niimi, M. Morota, D. H. Wei, C. Deranlot, M. Basletic, A. Hamzic, A. Fert, 341
- 318 and Y. Otani, *Phys. Rev. Lett.* **106**, 126601 (2011). 342
- 319 <sup>22</sup>J. Cramer, T. Seifert, A. Kronenberg, F. Fuhrmann, G. Jakob, M. Jourdan, T. 343
- 320 Kampfrath, and M. Kläui, *Nano Lett.* **18**, 1064 (2018). 344
- 321 <sup>23</sup>U. H. Pi, K. W. Kim, J. Y. Bae, S. C. Lee, Y. J. Cho, K. S. Kim, and S. Seo, *Appl.* 345
- 322 *Phys. Lett.* **97**, 162507 (2010). 346
- <sup>24</sup>M. Hayashi, J. Kim, M. Yamanouchi, and H. Ohno, *Phys. Rev. B* **89**, 144425 323
- (2014). 324
- <sup>25</sup>T. Schulz, K. Lee, B. Krüger, R. Lo Conte, G. V. Karnad, K. Garcia, L. Vila, B. 325
- Ocker, D. Ravelosona, and M. Kläui, *Phys. Rev. B* **95**, 224409 (2017). 326
- <sup>26</sup>O. Boulle, G. Malinowski, and M. Kläui, *Mater. Sci. Eng.* **R72**, 159 327
- (2011). 328
- <sup>27</sup>A. V. Khvalkovskiy, V. Cros, D. Apalkov, V. Nikitin, M. Krounbi, K. A. 329
- Zvezdin, A. Anane, J. Grollier, and A. Fert, *Phys. Rev. B* **87**, 020402 (2013). 330
- <sup>28</sup>A. Thiaville, S. Rohart, É. Jué, V. Cros, and A. Fert, *Europhys. Lett.* **100**, 57002 331
- (2012). 332
- <sup>29</sup>J. M. D. Coey, *Magnetism and Magnetic Materials* (Cambridge University 333
- Press, 2010). 334
- <sup>30</sup>E. C. Stoner and E. P. Wohlfarth, *Philos. Trans. R. Soc. London, Ser. A* **240**, 335
- 599 (1948). 336
- <sup>31</sup>R. A. Khan, P. M. Shepley, A. Hrabec, A. W. J. Wells, B. Ocker, C. H. Marrows, 337
- and T. A. Moore, *Appl. Phys. Lett.* **109**, 132404 (2016). 338
- <sup>32</sup>E. Martinez, S. Emori, and G. S. D. Beach, *Appl. Phys. Lett.* **103**, 072406 (2013). 339
- <sup>33</sup>S. Pizzini, J. Vogel, S. Rohart, L. D. Buda-Prejbeanu, E. Jue, O. Boulle, I. M. 340
- Miron, C. K. Safeer, S. Auffret, G. Gaudin, and A. Thiaville, *Phys. Rev. Lett.* 341
- 113**, 047203 (2014). 342
- <sup>34</sup>X. Ma, G. Yu, C. Tang, X. Li, C. He, J. Shi, K. L. Wang, and X. Li, *Phys. Rev.* 343
- Lett.* **120**, 157204 (2018). 344
- <sup>35</sup>A. Belabbes, G. Bihlmayer, F. Bechstedt, S. Blügel, and A. Manchon, *Phys. Rev.* 345
- Lett.* **117**, 247202 (2016). 346